EARTH SURFACE PROCESSES AND LANDFORMS
Earth Surf. Process. Landforms **45**, 1141–1154 (2020)

Published online 26 February 2020 in Wiley Online Library
(wileyonlinelibrary.com) DOI: 10.1002/esp.4783

Estuarine biofilm patterns: Modern analogues for Precambrian self-organization

Roeland C. van de Vijsel,[1,2]* Jim van Belzen,[1,3] Tjeerd J. Bouma,[1,4] Daphne van der Wal,[1,5] Valentina Cusseddu,[6] Sam J. Purkis,[7] Max Rietkerk[8] and Johan van de Koppel[1,2]

[1] NIOZ Royal Netherlands Institute for Sea Research, Department of Estuarine and Delta Systems, and Utrecht University, PO Box 140, Yerseke, NL-4400 AC, The Netherlands
[2] Groningen Institute for Evolutionary Life Sciences, University of Groningen, PO Box 11103, Groningen, NL 9700 CC, The Netherlands
[3] Ecosystem Management Research Group, University of Antwerp, Universiteitsplein 1, 2610 Wilrijk, Belgium
[4] Department of Physical Geography, Faculty of Geosciences, Utrecht University, 3508 TC, Utrecht, The Netherlands
[5] Faculty of Geo-Information Science and Earth Observation (ITC), University of Twente, PO Box 217, 7500 AE, Enschede, The Netherlands
[6] Dipartimento di Scienze della Natura e del Territorio, Polo Bionaturalistico, University of Sassari, Via Piandanna 4, 07100 Sassari, Italy
[7] CSL – Center for Carbonate Research, Department of Marine Geosciences, RSMAS, University of Miami, 4600 Rickenbacker Causeway, Miami, FL 33149, USA
[8] Copernicus Institute, Department of Environmental Sciences, Utrecht University, PO Box 80115, 3508 TC, Utrecht, The Netherlands

Received 27 May 2018; Revised 15 November 2019; Accepted 25 November 2019

*Correspondence to: Roeland C. van de Vijsel, NIOZ Royal Netherlands Institute for Sea Research, Department of Estuarine and Delta Systems, and Utrecht University, PO Box 140, Yerseke NL-4400 AC, The Netherlands. E-mail: roeland.van.de.vijsel@nioz.nl

Data and scripts can be found under https://doi.org/10.25850/nioz/7b.b.m

ESPL
Earth Surface Processes and Landforms

ABSTRACT: This field and laboratory study examines whether regularly patterned biofilms on present-day intertidal flats are equivalent to microbially induced bedforms found in geological records dating back to the onset of life on Earth. Algal mats of filamentous *Vaucheria* species, functionally similar to microbial biofilms, cover the topographic highs of regularly spaced ridge–runnel bedforms. As regular patterning is typically associated with self-organization processes, indicators of self-organization are tested and found to support this hypothesis. The measurements suggest that biofilm-induced sediment trapping and biostabilization enhance bedform relief, strength and multi-year persistence. This demonstrates the importance of primitive organisms for sedimentary landscape development. Algal-covered ridges consist of wavy-crinkly laminated sedimentary deposits that resemble the layered structure of fossil stromatolites and microbially induced sedimentary structures. In addition to layering, both the morphological pattern and the suggested formation mechanism of the recent bedforms are strikingly similar to microbialite strata found in rock records from the Precambrian onwards. This implies that self-organization was an important morphological process in times when biofilms were the predominant sessile ecosystem. These findings furthermore emphasize that self-organization dynamics, such as critical transitions invoking ecosystem emergence or collapse, might have been captured in fossil microbialites, influencing their laminae. This notion may be important for paleoenvironmental reconstructions based on such strata. © 2019 The Authors. Earth Surface Processes and Landforms published by John Wiley & Sons Ltd

KEYWORDS: biogeomorphology; long-term morphodynamics; ridges and runnels; bedforms; biostabilization; biofilms; algal mats; self-organization; autogenic dynamics; stromatolites; microbially induced sedimentary structures; microbialites; sedimentary record; paleoenvironment

Introduction

The importance of biological stabilization and strengthening of sediments in tidal depositional environments has been widely acknowledged (e.g. Widdows *et al.*, 2004; Le Hir *et al.*, 2007; Stal, 2010; Grabowski *et al.*, 2011). Biostabilizers are biota that enhance sediment stability by reducing sediment erodibility (e.g. Paterson, 1989, 1994) and increasing shear strength (e.g. Pestrong, 1969). They often decelerate the flow locally, which increases sedimentation, and incorporate sediment into their matrix while growing upwards. For microbial mats, Noffke (2010) categorizes these processes as biostabilization (protection against erosion), baffling (sieving grains from the water), trapping (sticking grains to the mat surface), binding (interweaving to form a mat) and growth (biomass increase). Biostabilizing organisms are found along the entire tidal range, from supratidal dune grasses (e.g. Durán and Herrmann, 2006) to intertidal salt marsh plants (e.g. Neumeier and Ciavola, 2004)

and mudflat micro- and macroalgal mats (e.g. Paterson, 1994; Sutherland *et al.*, 1998; Blanchard *et al.*, 2000; Romano *et al.*, 2003; Stal, 2010), and from intertidal and subtidal seagrass meadows (e.g. Fonseca, 1989; Christianen *et al.*, 2013; James *et al.*, 2019) to shellfish reefs (e.g. Widdows *et al.*, 2002). Sediment stability crucially determines functioning and development of the landscape and its ecosystem. For instance, mudflat accretion/erosion dynamics are closely linked to biofilm presence (Widdows and Brinsley, 2002) and creek bank stabilization by vegetation shapes tidal network morphology (Kearney and Fagherazzi, 2016). Moreover, ecosystem establishment depends on stable substrates (e.g. Brinkman *et al.*, 2002; Hu *et al.*, 2015; Cao *et al.*, 2018) or sufficient water clarity (e.g. Newell and Koch, 2004; van der Heide *et al.* 2007). Even global climate is impacted by organisms that bind, accumulate and consequently are buried by sediment, as they sequester carbon (e.g. Chmura *et al.*, 2003; McLeod *et al.*, 2011; Atwood *et al.*, 2015). Thus, biostabilizers affect the very foundations of tidal sedimentary landscapes.

Earth's geological record boasts ample evidence for long-lived sediment biostabilization. Microbialites (Burne and Moore, 1987) represent a substantial part of the sedimentary rock record from the Archean onwards (e.g. Bosak *et al.*, 2013; Noffke and Awramik, 2013). These deposits are formed by microbial communities, thin biofilms that can develop further into cohesive microbial mats, which interact with water flow and sediment transport by excreting glue-like extracellular polymeric substances (EPS) or forming a dense mesh of filaments (Stal and Caumette, 1994; Stal, 2010). In siliciclastic depositional environments, these biophysical interactions can result in often laminated, microbially induced sedimentary structures (e.g. Noffke, 1999; Noffke *et al.*, 2001). In carbonate-rich environments, microbial mats may also precipitate minerals, forming microbialites such as the pronouncedly laminated stromatolites, with layers typically micrometres to millimetres thick (e.g. Riding, 2000, 2011; Bosak *et al.*, 2013; Noffke and Awramik, 2013). There is mounting evidence for the important contribution of microbial mats on sediment stability (e.g. *Microcoleus chtonoplastes* literally means 'soil former') and hence the formation of such structures (e.g. Noffke, 1999; Schieber, 1999; Noffke *et al.*, 2007), although lamination, a key aspect of many microbialites, might also arise due to abiotic sedimentary processes (e.g. Grotzinger and Rothman, 1996; Grotzinger and Knoll, 1999; Brasier, 2011). Microbialites could grow for up to thousands of years, range in spatial scale from millimetres to kilometres and are often clearly spatially patterned, with pattern wavelengths ranging from the order of 1 cm to 10 m (e.g. Bosak *et al.*, 2013; Noffke and Awramik, 2013; Mariotti *et al.*, 2014). This patterning is often regular, e.g. for the Holocene stromatolites of Shark Bay (Australia) and the Bahamas (e.g. Logan, 1961; Andres and Reid, 2006; Bosak *et al.*, 2013), but not always (e.g. Noffke, 1999, 2008). Fossil microbialites, given their well-preserved layer sequences and abundance in the geological record, are valuable for paleoenvironmental reconstructions (Logan *et al.*, 1964; Jerzykiewicz and Sweet, 1988; Harzhauser *et al.*, 2014; Lettéron *et al.*, 2017). Despite the valuable information about formation mechanisms and environmental conditions that can be deduced from spatial patterns (e.g. Pascual and Guichard, 2005; Rietkerk and van de Koppel, 2008), microbialite patterns and their implications for paleo-reconstructions have received relatively little scientific interest.

Present-day biofilms and their bedforms may serve as analogues to Precambrian and Phanerozoic microbialites (e.g. Noffke, 2008; Noffke *et al.*, 2013). Although stromatolites declined rapidly after the Precambrian, likely due to the evolution of burrowing and grazing animals (e.g. Walter and Heys, 1985) and changes in sea water chemistry (e.g. Stal, 2010), microbially induced sedimentary structures did not experience such a drastic drop in numbers and sediment-sculpting biofilms are still ubiquitous on present-day tidal flats (e.g. Noffke, 2008). These communities of primitive unicellular organisms can potentially cover and stabilize large intertidal areas rapidly, typically within one growth season (e.g. Noffke and Krumbein, 1999; de Brouwer *et al.*, 2000). Just like their ancestors, these modern biostabilizers commonly exhibit spatial patterning (e.g. Noffke, 1999; Blanchard *et al.*, 2000; de Brouwer *et al.*, 2000; Lanuru *et al.*, 2007; Weerman *et al.*, 2010, 2012). Regular spatial patterns can be induced by scale-dependent feedbacks, whose sign and magnitude depend on distance (Rietkerk and van de Koppel, 2008). Regular patterns in biofilms (Weerman *et al.*, 2010) and salt marsh vegetation (Temmerman *et al.*, 2007) are thought to result from scale-dependent feedbacks in which water flow diverges away from topographic elevations. These elevations are then preferentially colonized and biostabilized, creating a local positive feedback. Flow convergence in surrounding topographic lows leads to increased inundation and shear stress and hence reduced biostabilization. Thus, this feedback is 'scale-dependent', as it is locally positive but has 'reversed sign' more distantly.

Although fairly similar morphologies are found in microbial mat-covered erosional remnants and uncovered erosional pockets, such bedforms are shaped by a runaway erosional disturbance, causing progressive pocket erosion in a formerly intact mat (Noffke, 1999, 2010; Noffke and Krumbein, 1999). Although this is a positive feedback process as well, it is markedly different from the previously explained scale-dependent feedback. This might explain why erosional remnants and pockets appear not to be clearly regularly patterned. In contrast, it is likely that regularly spaced intertidal ridge–runnel bedforms do arise from a scale-dependent feedback (although this term is not used in the ridge–runnel literature): spontaneous flow instabilities are amplified by flow convergence above and net erosion of poorly drained runnel sediments and net sedimentation related to flow divergence and higher sediment stability above well-drained ridges (e.g. Allen, 1987; Gouleau *et al.*, 2000; O'Brien *et al.*, 2000; Williams *et al.*, 2008; Carling *et al.*, 2009). Although this feedback can be purely geophysical, ridge colonization by biostabilizers might amplify the stability contrast (ridge vs runnel) and hence the feedback (e.g. Blanchard *et al.*, 2000; Lanuru *et al.*, 2007; Williams *et al.*, 2008; Weerman *et al.*, 2010; Fagherazzi *et al.*, 2013).

The emergence of large-scale structure or patterning from initial disorder due to local (scale-dependent) interactions is known as spatial self-organization (Rietkerk and van de Koppel, 2008); a Turing instability (Turing, 1952) is one of the mechanisms behind pattern emergence. Self-organization dynamics are typically nonlinear, possibly invoking bistability (e.g. degraded vs restored ecosystem state), with drastic, critical transitions between states (e.g. May, 1977; van de Koppel *et al.*, 2001, 2005; Rietkerk *et al.*, 2002; Weerman *et al.*, 2010; Scheffer *et al.*, 2012; Liu *et al.*, 2014b). Such critical transitions might also be more stepwise in multi-stable systems, allowing a range of different pattern wavelengths (Bastiaansen *et al.*, 2018). Thus, it is essential, for example for paleo-reconstructions based on microbialites, to understand how their patterns are formed, as self-organized regularly patterned systems may behave very differently from disturbance-driven irregularly patterned systems (e.g. Noffke, 1999; Guichard *et al.*, 2003; Pascual and Guichard, 2005; Weerman *et al.*, 2012).

Present-day self-organized biofilm bedforms (Weerman *et al.*, 2010) show strong resemblance, both in morphology and underlying processes, to regularly patterned, dome-shaped stromatolites (e.g. Logan, 1961). Yet, although self-organization

in stromatolites has been suggested before (e.g. Petroff *et al.*, 2010; Brasier, 2011; Tice *et al.*, 2011), the possible implications thereof have not been broadly explored yet (Purkis *et al.*, 2016). Possibly, the hypothesis of self-organization has not received much attention because an essential and defining aspect of many microbialites – lamination – is not always found or evident in modern mudflat bedforms (e.g. Weerman *et al.*, 2010). Lamination, principally a consequence of abiotic sedimentary processes (e.g. Gouleau *et al.*, 2000; Williams *et al.*, 2008; Carling *et al.*, 2009), can be enhanced by long-term biostabilization with temporally variable binding rates (Williams *et al.*, 2008). These biogenic effects can be preserved as wavy-crinkly layering (Horodyski, 1982; Schieber, 1999; Riding, 2011; Noffke *et al.*, 2007; Sarkar *et al.*, 2016). Yet, instead of long-term biostabilization, many previous studies have focused on environments with strong seasonality, thus emphasizing the short-term aspects of modern biofilms (de Brouwer *et al.*, 2000; Widdows and Brinsley, 2002; Le Hir *et al.*, 2007; Weerman *et al.*, 2010, 2011, 2012). As microbial biofilms form a protective 'skin layer' on the sediment, the underlying sediment regains its higher, abiotic erodibility as soon as the biofilm is eroded by grazing, hydrodynamics or both (de Brouwer *et al.*, 2000; van de Koppel *et al.*, 2001; Widdows and Brinsley, 2002; Le Hir *et al.*, 2007; Weerman *et al.*, 2010, 2011, 2012), such that sedimentary deposits characterized by well-defined laminae cannot develop. Sediment lamination has been reported on mudflats where ridge and runnel bedforms persist multi-annually, but without consideration of the influence of biofilms or similarities with stromatolites (Gouleau *et al.*, 2000). To answer the question of whether the formation and regular patterning of many layered microbialites could be self-organized, modern analogues are needed which are morphologically and mechanistically similar, but which also withstand biophysical seasonality enough to construct long-lasting, laminated deposits.

Mats composed of simple multicellular biostabilizers such as macroalgae might have an even stronger potential to form such layered deposits. Primitive filamentous macroalgae such as *Enteromorpha* sp. (e.g. Raffaelli *et al.*, 1999; Widdows and Brinsley, 2002; Romano *et al.*, 2003; Le Hir *et al.*, 2007) and *Vaucheria* sp. (e.g. Simons, 1975; Gallagher and Humm, 1981; Wilcox, 2012) have been reported to persist multi-annually (Romano *et al.*, 2003). Moreover, all biophysical interactions characterizing microbially induced sedimentary structures (Noffke *et al.*, 2001) have also been described for *Vaucheria* mats. *Vaucheria* baffles, traps and binds sediment (Black, 1933; Skowroński *et al.*, 1998) in its dense mesh of filaments that can penetrate the soil down to 4–6 cm and grow upwards when buried (Gallagher and Humm, 1981), effectively biostabilizing (Webber, 1967; Paterson, 1994) and forming thick and patchy organosedimentary mats (Simons, 1975; Gallagher and Humm, 1981; Wilcox, 2012). However, the impact of such mats on long-term morphodynamics, sediment lamination or bedform patterning has not been explored in detail. Although these mats are not biofilms in their strictest definition (i.e. they are not microbial and do not excrete large amounts of EPS; e.g. Stal, 2010), their primitive form, rapid and sheet-like growth, and distribution along the entire salinity range (Simons, 1975) makes them similar to microbial biofilms. Multicellular algae like *Vaucheria* were rare in the Precambrian, but not absent (Butterfield, 2004). For the purpose of this study, the definition of biofilms will therefore be slightly broadened (following Fagherazzi *et al.*, 2013) to include functionally similar mats composed of multicellular macroalgae. Do such mats create laminated and patterned bedforms, contributing to long-term estuarine morphodynamics just like cyanobacteria and other microbialite-building organisms did from the Precambrian onwards (Noffke, 1999, 2010; Noffke and Krumbein, 1999; Riding, 2011)?

This study reports on present-day intertidal ridge–runnel bedforms that seem regularly spaced and persistent for multiple years, with long-lived *Vaucheria* mats covering topographic highs (Figure 1). These algal mats will also be referred to as 'biofilms' throughout this study. These metre-scale bedforms are observed on intertidal flats in the Schelde estuary in Belgium, close to the Dutch border (see Figures SI1 and SI5). *Vaucheria* bedforms are sometimes more dome-shaped (Figure 2), broadly resembling the morphology of many stromatolites (Logan, 1961; Andres and Reid, 2006). These observations raise multiple questions. Are the *Vaucheria* bedforms indeed regularly patterned and could self-organization explain this? How long do the algal and topographic patterns persist? Are the bedforms laminated, resembling layered microbialites? To address these questions, specific indicators of self-organization due to biophysical scale-dependent feedbacks will be tested, including bedform regularity and orientation, pattern formation history and local biostabilization by algae. Moreover, pattern persistence will be quantified using remote sensing data. Finally, the bedforms will be examined for wavy-crinkly lamination, a key property of many microbialites.

Methods

Study area

Field measurements were done on the intertidal flat of Ketenisse (51.285063°N, 4.312082°E), in the far upstream mesohaline zone of the Schelde estuary, with water salinity fluctuating around 3.6 ppt in 2006 (van den Neucker *et al.*, 2007). This coastal realignment site, consisting of formerly embanked agricultural land, was de-embanked in 2002 to restore it as a mudflat and has been accreting estuarine sediments ever since. The mudflat is currently embanked on the south and west side, with salt marsh vegetation (e.g. *Bolboschoenus maritimus, Phragmites australis*) in front, and is bordered by the estuarine channel along the north-to-east border (Figure SI1). Early 2003, MLW, MHW and MHWS were at respectively −2.3, +3.0 and +3.4 m relative to mean sea level (MSL); at that time the restored mudflat was elevated from about 1.9 to 2.3 m above MSL (van den Neucker *et al.*, 2007).

Figure 1. Regular bedforms with ridges covered by *Vaucheria* algal mats and runnels without algal cover. Picture taken on 26 August 2016 at Ketenisse (around 51.284836°N, 4.312567°E), see also Figure SI1. The Schelde estuary is visible in the background. [Colour figure can be viewed at wileyonlinelibrary.com]

Figure 2. *Vaucheria* bedforms on Galgeschoor, Schelde estuary (around 51.321231°N, 4.282745°E), see also Figure SI1. Photograph (date unknown) included with permission and courtesy of Frank Wagemans. [Colour figure can be viewed at wileyonlinelibrary.com]

In 2016, the Ketenisse mudflat reached up to about 3.0 m above MSL (Figure SI1). Between 2003 and 2006, the average bed slope was 0.002 m m^{-1} and the median grain size varied between about 27 and 76 μm (van den Neucker *et al.*, 2007). Already in 2003, the first year after de-embankment, *Vaucheria*-covered ridges and bare, ca. 10 cm-deep runnels were observed (van den Neucker *et al.*, 2007). *Vaucheria* bedforms (Figure 1, photo taken in August 2016) were still found on large parts of the mudflat in 2018. From visual inspection in the field between 2015 and 2017, it seems that these ridges and runnels are elongated along the direction of downhill drainage flow. It also appears that some of the runnels are somewhat deeper and streamwise more continued (i.e. more similar to drainage creeks bordered by creek levees instead of runnels bordered by ridges). This is also observed elsewhere (Gouleau *et al.*, 2000; O'Brien *et al.*, 2000; Whitehouse *et al.*, 2000). The ridges and creek levees are covered by algae, primarily *Vaucheria*, while runnels and creeks are barely covered. Contrary to diatom-stabilized bedforms, which tend to be spatially regular but are often seasonally ephemeral (de Brouwer *et al.*, 2000; Weerman *et al.*, 2010, 2012), or to more persistent but less regular erosional remnants and pockets (Noffke and Krumbein, 1999), it appears that the *Vaucheria* bedforms are spatially regular (Figure 1) as well as persistent for many consecutive years, taking aside periods of extreme cold, heat or drought (Figure SI9).

Remote sensing techniques

In order to quantify the spatial and temporal characteristics of algal pattern and bedforms on the Ketenisse mudflat, an area of approximately 50 × 50 m (around 51.285063°N, 4.312082°E; Figure SI1) was marked with six small poles in August 2015. The poles were firmly anchored in the sediment and georeferenced with an RTK-dGPS (Leica Viva GNSS GS12 receiver with CS15 controller). This delimited area was left untouched and was analysed repeatedly over the course of time, using several remote sensing techniques.

Bedform geometry and temporal dynamics were measured with a tripod-mounted 3D terrestrial laser scanner (RIEGL VZ400). By emitting a laser beam, the rotating scanner creates a three-dimensional point cloud of the sediment surface. To georeference this point cloud, reflectors (5 cm diameter, RIEGL) were mounted on the six poles surrounding the study area. The 50 × 50 m area was scanned from at least three different vantage points to avoid shadowing effects due to surface topography. Each scan position was chosen such that at least four reflectors were captured; at least three overlapping reflectors were used to merge separate scans. Raw scanner data was processed using RiScan Pro (RIEGL) to obtain georeferenced x, y, z-coordinates (x, y horizontal; z vertical). All subsequent post-processing steps were achieved using Matlab (MathWorks, Inc.). Using linear interpolation, this x, y, z-point cloud was gridded onto a regular horizontal grid with 10 cm grid spacing to obtain a digital elevation model (DEM). To accelerate the computation time while retaining precision, interpolation was conducted with random subsamples of, on average, 50 x, y, z-points per grid cell. Bed-level elevation is expressed in metres above NAP (Amsterdam Ordnance Datum, roughly coinciding with mean sea level in Amsterdam, The Netherlands). To obtain relative bed-level elevation, the background elevation profile $S_N(x, y)$ of the form

$$S_N(x,y) = \sum_{i=0}^{N}\left(a_{ii}\, x^i \sum_{j=0}^{N-j} a_{ij} y^j\right)$$

with polynomial order N and constants a was calculated by regression and subtracted from the total elevation profile. Here, $N = 4$ was chosen as this gave higher R^2 than $N = 2$ or 3. As the delimited 50 × 50 m area was not exactly rectangular, a 44 × 49.5 m rectangular area was selected within the 50 × 50 m area (44 m south-to-north, 49.5 m west-to-east). The northward direction can be considered 'downslope' within this area, as the area–mean background surface gradient ∇S_N was oriented 359.05° from the north in August 2015. For a comparison of bedform to algal pattern (discussed below), three DEMs (11 August 2015, 13 December 2016 and 19 September 2017) were used.

Aerial photos were taken, to analyse algal mat coverage and correlate this with bed level. To make a year-on-year comparison, aerial photos acquired in 2015 (11 August), 2016 (13 December) and 2017 (19 September) are considered. The photos were captured with a DJI Inspire 1 drone with Zenmuse X3 gimbal and camera, with sufficient overlap to make an orthophoto. The photos were stitched together using Agisoft PhotoScan Pro to obtain an orthomosaic with a resolution of 1.75 cm (2015), 0.98 cm (2016) or 1.3 cm (2017). Four white reference plates (Figure SI9b) were placed in the field adjacent to the corner poles and georeferenced with the RTK-dGPS. In Matlab, either these four reference plates or the outermost four reference poles were used as control points to co-register the non-referenced orthomosaic to the georeferenced DEM. Each orthophoto mosaic was geometrically transformed and aligned with the DEM (i.e. with 10 cm grid spacing) to allow for a grid cell-wise

comparison. The algal pattern within the 44 × 49.5 m focus area was quantified using the visible-band difference vegetation index (VDVI) (Du and Noguchi, 2017), based on the image's green (G), blue (B) and red (R) pixel values:

$$\mathrm{VDVI} = (2G - B - R)/(2G + B + R)$$

The relative VDVI profile was computed by regression of the background profile $S_4(x, y)$ and subtraction from the total VDVI profile; this was done to correct for spatially large-scale spectral imbalances in the orthomosaic, hence to retain the smaller-scale algal pattern.

Algal presence farther back in time than the available laser scan and drone data was quantified from aerial images of the 44 × 49.5 m area obtained with Google Earth Pro (© 2016 Google Inc.). These images were acquired for 2004 (8 June), 2009 (31 August), 2012 (4 September), 2013 (7 July), 2015 (1 October) and 2017 (24 September). The original photos had a resolution of approximately 1.8 cm and were also geometrically transformed and aligned with a rectangular 10 cm-resolution grid. VDVI values were computed and a fourth-order background profile was regressed and subtracted to obtain relative VDVI values.

To test if the spatial algal pattern overlaps with the topographic pattern and whether this correlation persists in time (possibly contributing to lamination), elementwise linear correlation (Pearson's r) was performed, using Matlab, for the DEMs and drone-derived VDVI maps acquired in 2015, 2016 and 2017. Since the residuals were not homogeneously distributed, p-values could not be computed directly from the linear correlation itself. Instead, p-values were computed by randomly permuting the elements of each DEM or VDVI matrix 1000 times, recomputing the correlation coefficient at each permutation and calculating the probability of obtaining an equal or more extreme r-value than the 'true' r by chance.

Two-dimensional auto-correlation and cross-correlation matrices of the DEMs and VDVI maps of 2015, 2016 and 2017 were computed to quantify pattern regularity (van de Koppel *et al.*, 2005; Weerman *et al.*, 2010, 2012; Cornacchia *et al.*, 2018) and persistence over time. To quantify spatial regularity (auto-correlation) and displacement (cross-correlation) in west-to-east orientation (resp. north-to-south orientation), the row vector running eastward from each matrix's centre (resp. the column vector running southward from each matrix's centre) was analysed. Wavelength is quantified as the correlation distance where spatial auto-correlation is maximal, after increasing from negative to positive values. To assess the statistical significance of the auto- and cross-correlations, random permutation (as described above) was applied; each DEM and VDVI matrix was permuted 100 times. The p-value was given by the probability of finding an equally or more extreme correlation for that specific correlation distance by random chance. Since the DEM and VDVI matrices had very different units, the correlation matrices were normalized, for plotting purposes, by division by their maximal value. The same procedure was applied to VDVI matrices derived from Google Earth images (Supplementary Information, Figure SI7).

To estimate how many of the runnels are slightly deeper (i.e. more similar to creeks), a histogram (1000 bins) was made of relative bed level in 2015. This frequency distribution is bimodal (representing ridges and runnels), with a longer tail (representing creeks) developing towards lower elevations, distinguished from the bimodal distribution by a 'bump'. This classification allows creek/runnel/ridge distinction in the DEM. From the same histogram (and similarly for 2016 and 2017), modal (i.e. most frequent) ridge-to-runnel elevation differences (a measure for bedform topographic amplitude) were computed as the difference between most frequent ridge elevation and most frequent runnel elevation.

Sediment lamination

Four sediment cores, each approximately 30–35 cm long and 7 cm in diameter, were taken on the Ketenisse mudflat (September 2016) to test the hypothesis that biofilm-covered bedforms consist of laminated deposits, while bare tidal flat does not. Two cores (referred to as 'SE'; 51.284800°N, 4.312494°E) were taken about 11 m southeast of the southeastern corner of the 44 × 49.5 m area. The other two (referred to as 'NE'; 51.285267°N, 4.312572°E), meanwhile, were cored about 13 m east of the northeastern corner of the study area. At both locations, one core was taken on an algal-covered creek levee, the other one in the bare runnel behind (as seen from the creek) the levee. In the lab, the cores were sliced in half lengthwise and an X-radiograph was taken (HP Faxitron Cabinet X-ray model 43805 N). The cores were radiated for 2.5 min with a 50 kV source at 61 cm distance between source and light-sensitive film (Konica Minolta Regius RC-300 cassette). These X-radiographs (resolution 0.085 mm) were digitalized and converted to grey-value matrices (pixel intensity ranging from 0 to 255) and a subset (25 cm from the surface downwards, 6 cm wide) was extracted to exclude boundary effects near the sides and bottom of each core. Relative X-radiograph profiles were computed by regression and subtraction of background profiles $S_4(x, y)$. In this way, larger-scale light intensity changes (e.g. due to the semicircular shape of the sliced core) were filtered out.

Sediment biostabilization

To test the assumption of sediment strengthening by *Vaucheria*, penetration resistance, a measure of bed compaction (Williams *et al.*, 2008) or algal mat binding, was measured for all the sediment cores taken on the Ketenisse mudflat. Nine sediment cores (PVC tube, diameter 12 cm, length 20 cm) were taken in June 2015; three cores at three sites. Per site, one core was taken on an algal-covered creek levee, one core nearby where the same creek levee was not visibly algal-covered and one core in the bare runnel behind it (i.e. away from the creek). The three sites were approximately spaced at 10 m intervals along the same creek, with the central coring site at 51.285131°N, 4.311331°E (Figure SI1). In the lab, penetration resistance was measured with an INSTRON Testing System controlled with INSTRON Bluehill 3 software. Due to technical issues, this lab analysis was delayed for 2 weeks. In the meantime, and so as to preserve their integrity and physical properties, the cores were kept in controlled conditions (Supplementary Information, SI6). As this analysis was done to study relative differences between the substrates, rather than absolute values, the influence of this delay is not considered important. Penetration resistance as a function of depth (upper 100 mm, increments of 0.17 mm) was measured, in the centre of the sediment cores, with a metal cone (frontal area 2 cm^2, tip angle 60°). Median penetration resistance was computed for each profile; further calculations were done with these medians. After testing for normality (Shapiro–Wilk normality test) and homoscedasticity (Levene's test) of the nine residuals, a two-way analysis of variance (ANOVA) was performed of the fitted linear model, with both substrate (runnel, bare levee, algal-covered levee) and location (sites 1–3) as fixed factors. Analyses and statistics were performed using R (http://www.R-project.org).

Results

Self-organization of algal pattern and bedforms

A regularly spaced and dashed algal pattern emerged seemingly spontaneously, as can be seen on aerial photos of the 44 × 49.5 m focus area on the Ketenisse mudflat (Figure 3). Although *Vaucheria* had already colonized this mudflat by 2003 (van den Neucker *et al.*, 2007) (i.e. shortly after this area was de-embanked to become intertidal), the first Google Earth image from 2004 shows no signs of colonization in the focus area yet. Aerial images do not exhibit regular patterning before 2012. Some irregular clustering in a west-to-east and northwest-to-southeast orientation is observed in 2004, however. In the next aerial image available in the time series (2009), the entire focus area is covered by algal patches, but they show no apparent regularity. By contrast, in 2012, 2013, 2015 and 2017, a regularly spaced algal pattern was present, with dominant wavelengths of 2.4, 2.6, 2.5 and 3.0 m, respectively, in an east-to-west direction, as quantified by the spatial auto-correlation ($p < 0.01$; Figure SI7a). No clear wavelength was detected in the north-to-south direction for 2012–2017. Background bed level $S_4(x, y)$ in 2015 sloped down towards the north. The algal pattern visible between 2012 and 2017 is therefore oriented streamwise. Thus, emergence of a flow-aligned regular algal pattern, apparently without pre-existing topographic structuring, is consistent with the hypothesis of self-organization due to scale-dependent feedbacks, with or without active biotic involvement.

Vaucheria bedform morphology

The algal pattern is in good accordance with the underlying topographic pattern (i.e. the ridges have algal cover and the runnels are bare). Apart from this being visible in the field (Figures 1 and 2), the association follows from elementwise linear correlation of laser scan-derived relative bed level with drone-derived relative VDVI within the focus area (Pearson's r = 0.488 for 11 August 2015, 0.552 for 13 December 2016, 0.384 for 19 September 2017; $p < 0.001$ for all three dates). Spatial auto-correlations ($p < 0.01$) of both relative bed level and relative VDVI (Figure 5a) confirm that bedform ridges are elongated along the direction of downstream drainage flow and are regularly spaced in the cross-flow (spanwise) direction. The dominant wavelength (i.e. distance of maximal correlation) in the cross-flow direction is 2.6, 2.6, 2.8 m for DEM 2015, 2016, 2017 respectively and 2.3, 2.4 m for VDVI 2015, 2016, respectively. When the algal pattern gradually starts broadening and fragmenting towards 2017 (Figures 3 and SI9a), a dominant wavelength can no longer be computed (i.e. the auto-correlation of VDVI 2017 has a maximum at 2.5 m but does not change sign). No clear wavelength (at least none smaller than 10 m) exists in the northward (downslope) direction for either the DEMs or drone-derived VDVI matrices from 2015, 2016 and 2017. Roughly every 6–8 m in the spanwise direction (in 2015), ridges are longer (more continuous) in the streamwise direction (i.e. more similar to creek levees) and the runnels they border are slightly deeper (i.e. more similar to drainage creeks). The modal ridge–runnel elevation difference is 5.3 cm in 2015, 5.2 cm in 2016 and 2.3 cm in 2017. In winter and during hot and dry summer periods, algal cover is substantially reduced, or sometimes not even visible. Between May and July 2017, it was visually observed that algal cover gradually shifted from the ridges to the (sides of the) runnels (Figure SI9a). By September 2017, however, the algae had started to recolonize the ridges. Further testing of the algal growth potential in bare sediments (van Belzen, 2018) revealed that *Vaucheria* spores were omnipresent and could grow everywhere in the field, including bare areas, given the right growth conditions (Supplementary Information, Figure SI3). Thus, the observations of regularly spaced ridge–runnel bedforms in combination with stronger *Vaucheria* growth potential on ridges are in agreement with the hypothesized biophysical scale-dependent feedback.

Multi-year pattern persistence

For several consecutive years, the regularly spaced algal mat pattern overlaps with the bedform pattern and remains at the same location on the Ketenisse mudflat. Between 2015 and

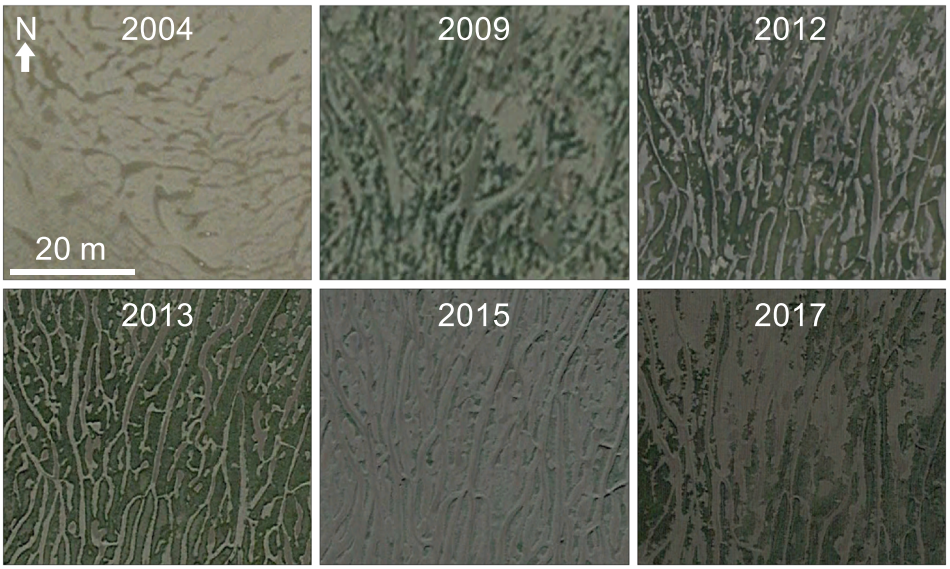

Figure 3. Algal pattern organization history between 2004 and 2017, retrieved from aerial images of the 44 × 49.5 m focus area (geometrically transformed, 10 cm resolution) on Ketenisse (51.285063°N, 4.312082°E). Green colour corresponds to algal cover. Aerial images © 2018 DigitalGlobe and © 2018 Aerodata International Surveys, obtained and adapted from Google Earth Pro, © 2016 Google Inc. [Colour figure can be viewed at wileyonlinelibrary.com]

2016, relative bedform topography stays largely in place (Pearson's r = 0.690, $p < 0.001$), as it does between 2016 and 2017 (r = 0.818, $p < 0.001$) and between 2015 and 2017 (r = 0.664, $p < 0.001$). In agreement with this topographic persistency and the preferred colonization of topographic highs (previous section), the VDVI patterns are significantly correlated year-on-year, although less strongly than the topography (VDVI 2015–2016, r = 0.250; 2016–2017, r = 0.114; 2015–2017, r = 0.137; all $p < 0.001$). The effects of the temporal algal relocation during summer 2017 (Figure SI9a) are still measurable in the 2017 VDVI data, such that this year correlates less strongly with 2015 and 2016. The persistence of algal pattern and bedform wavelength can also be seen from the auto- and cross-correlation profiles (Figure 5). In the cross-flow direction, cross-correlations follow a similar profile as auto-correlations, emphasizing that between subsequent years, the regular topographic and algal patterns mostly stay in the same location. The 0.3 m shift in VDVI cross-correlation between 2016 and 2017 reflects the after-effect of the temporal algal relocation (Figure SI9a). Between 2015 and 2017, the entire 44 × 49.5 m focus area gradually accretes sediment over the course of time and rises about 2.9 cm year^{-1} along its northern edge (Figure SI2) and about 4.0 cm year^{-1} along its southern edge (Figure 4). Bedforms are best preserved on the southern edge of the focus area (as also observed for the algal pattern, Figure 3) and seem to gradually flatten out on the northern edge. Long-term persistence is also evident from the auto- and cross-correlations computed for the Google Earth time series (Figures 3 and SI7): the algal pattern does not change much in wavelength between years and stays mostly in the same location. Hence, overall, the regularly spaced algal pattern and underlying bedforms are persistently present for multiple consecutive years, despite significant accretion rates.

Linking sediment lamination and biostabilization

Algal-covered creek levees are horizontally wavy-crinkly layered and have more stable sediments than bare runnels, which do not exhibit such lamination. Layering is clearly visible in the X-radiograph of the algal core taken around the southeastern (SE) edge of the focus area (Figure 6). Broad dark and light bands alternate with about 4.5 cm vertical spacing, as shown by the spatial auto-correlations (Figure SI4). Finer millimetre-scale wavy-crinkly laminae are also visible, mostly within the broad dark bands of this core (Figure SI8). Although some of these undulations appear to coincide with burrows (a, b in Figure SI8), crinkly textures are also observed away from bioturbation tracks (c, d). The ca. 1 cm wavelengths of the crinkles are of roughly the same scale as the tufted, wavy *Vaucheria* mat texture (Figure 1). Assuming 4 cm year^{-1} accretion, the broad dark bands with finer crinkles, at between 12 and 20 cm depth, date from between 2011 and 2013, coinciding with the Google Earth images that exhibit most pronounced algal cover (Figure 3). In the northeastern (NE) algal core, broad (4.6 cm spacing, Figure SI4) and fine (millimetre-scale) lamination are vaguely visible, yet less evident than in the SE-algal core. Broad- and fine-scale lamination are even more vague in the sediment cores taken in bare runnels (both on the NE and SE side). Penetration resistance (Figure 7) of *Vaucheria*-covered creek levees (194 kPa, i.e. least square mean of the three profile medians) was significantly higher than that of bare creek levees (89.3 kPa) and bare runnels (13.7 kPa), as follows from pairwise comparisons of the least square means (all $p <$ 0.0001, adjusted with the Tukey method). All substrates have significant effect (two-way ANOVA, $p < 0.001$), whereas sites do not. Thus, the data show concurrence of algal cover, stable sediments and wavy-crinkly laminae.

Discussion

Present-day intertidal flats are often typified by regularly patterned bedforms shaped by biofilms, highlighting that spatial self-organization is an important intertidal landscape-building process. Strikingly, similarly regularly spaced biofilm bedforms are abundantly found in the fossil record as laminated microbialites, dating back to the Precambrian. Yet, modern biofilm patterns are often ephemeral, which inhibits the build-up of sedimentary lamination. This leaves the question of to what extent self-organization has shaped shallow-marine landscapes throughout Earth's geological history. This study highlights that biofilm-forming, primitive biostabilizers can stimulate self-organization of modern mudflats into regularly patterned, multi-annually persistent and hence internally laminated ridge and runnel bedforms. Flow deceleration and trapping, binding

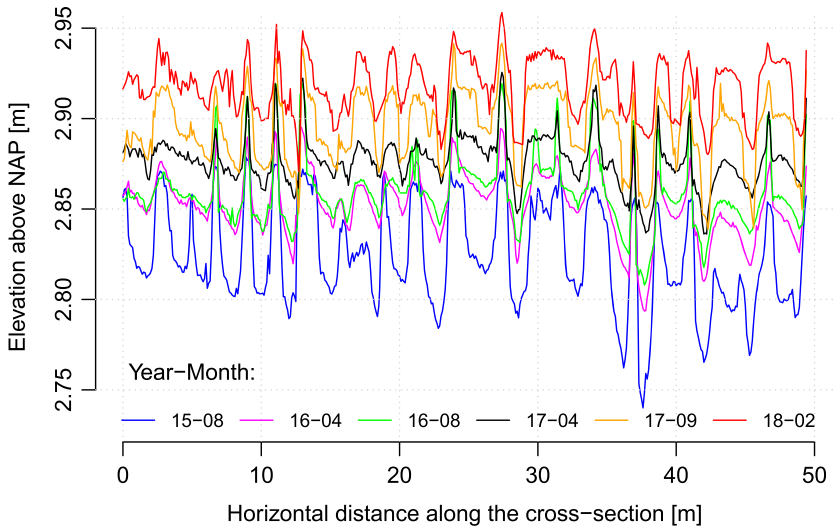

Figure 4. Bottom elevation profiles along the southern edge (i.e. 20 cm north of the southern edge) of the 44 × 49.5 m focus area on Ketenisse. Elevations derived from *in-situ* laser scan measurements; NAP is roughly mean sea level. Different lines denote different moments in time at which the elevation was measured. The bedform pattern is persistent, despite gradual sediment accretion. [Colour figure can be viewed at wileyonlinelibrary.com]

and biostabilization of ridge sediments by mats of the filamentous macroalgae *Vaucheria* sp. (functionally similar to microbial biofilms) likely boosts the formation and multi-year persistence of metre-scale ridge–runnel topography and enhances layered deposition, forming typical wavy-crinkly laminae. Both the crinkled layers and regular bedform morphologies are strikingly similar to modern and ancient microbialites, ranging in morphology from planar microbially induced sedimentary structures to dome-shaped stromatolites. This study therefore suggests that spatial self-organization, due to biophysical scale-dependent feedbacks, might be an important process shaping inter- and subtidal ecosystems, not only in the present, but dating back to the Precambrian, when biofilms were the predominant benthic ecosystem on the planet.

Algal/topographic pattern regularity and indications of self-organization

Multiple measurements indicate that the observed algal bedforms are likely self-organized, as explained below. Regularly spaced algal-covered ridges and bare runnels are observed from 2012 onwards (Figures 3, 4, 5 and SI7). Yet, such structuring appears absent prior to 2012. The irregular clustering observed in 2004 (Figure 3), with different orientation than the pattern from 2012 onwards, probably reflects drainage topography, given the underlying terrain slope in 2004 (see figure 5.14 in van den Neucker *et al.*, 2007). In 2009, algal cover (and hence also topography, given the positive correlation found between cover and elevation) was irregular (Figure 3). Hence, spatial regularity arises from seemingly disordered initial conditions, which is consistent with self-organization principles (e.g. Rietkerk and van de Koppel, 2008). This suggests that internal feedbacks are important structuring processes. This study indicates how such a scale-dependent feedback loop might work. Algal mats are preferentially found on elevated ridges (Figure 1), despite algal spore presence across the tidal flat (Figure SI3). Ridge sediments, in turn, are more stable (Figure 7), most likely due to biostabilization (Webber, 1967; Paterson, 1994), combined with better drainage and lower shear stress compared to runnels (e.g. Gouleau *et al.*, 2000; O'Brien *et al.*, 2000; Williams *et al.*, 2008; Carling *et al.*, 2009). This mechanism, as well as the observed flow-alignment of the *Vaucheria* bedforms (Figures 5 and SI1) is consistent with the biophysical scale-dependent feedback described by Temmerman *et al.* (2007) and Weerman *et al.* (2010). The idea of a feedback loop is further supported by the fact that algal bedforms retain their wavelength and amplitude for several years, despite rapid sediment accumulation (Figures 3–5 and SI7): without site-dependent sediment erosion and stabilization, runnels (or creeks) would be expected to fill up and/or ridges (or creek levees) to flatten out (e.g. Williams *et al.*, 2008). Indeed, the observed bedforms are significantly flattened out in autumn 2017, following a hot summer in which it was visually observed that algal cover temporarily shifted from the ridges to (the sides of) the runnels (Figure SI9a), which is likely the result of heat or desiccation stress. It is tempting to assume a causal relation, yet a multi-annual time series (encompassing both topography and algal distribution) with higher temporal resolution is required to more firmly support the notion that biofilm cover directly affects bedform geometry. In-depth study of the seasonal changes in algal cover and bedform morphology, as well as zonation along the tidal range, could for example be quantified with the biotic modification index introduced by Noffke and Krumbein (1999).

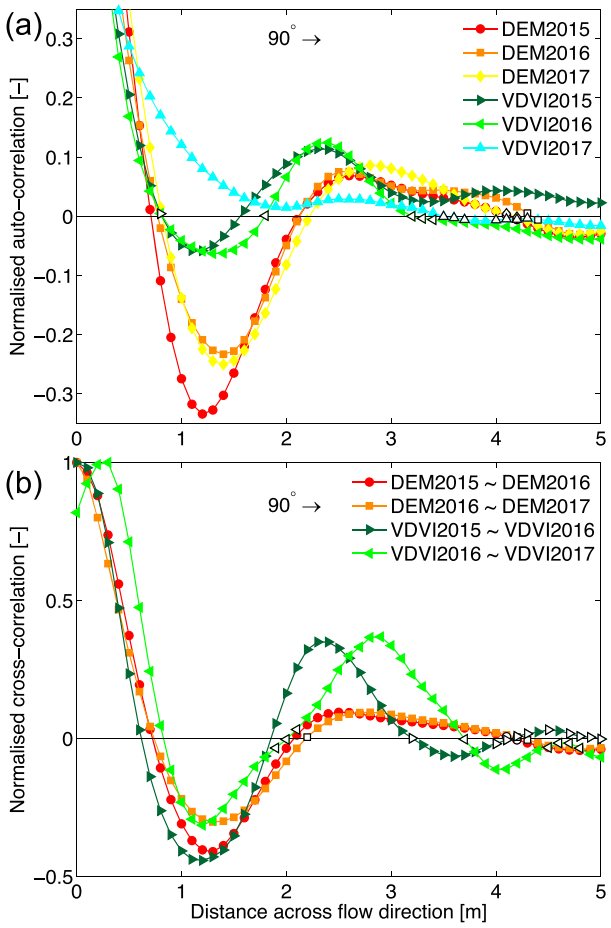

Figure 5. Normalized spatial auto-correlations (a) and cross-correlations (b) of laser scan-derived relative bed level (DEM) and drone-derived relative green intensity (VDVI) in 2015, 2016 and 2017, computed along the cross-flow (west-to-east) direction within the 44 × 49.5 m focus area on Ketenisse. White markers indicate non-significant data points ($p \geq 0.01$), coloured markers are statistically significant ($p < 0.01$) based on 100 random permutations. Each correlation profile is afterwards normalized by dividing it by its maximum value, for visibility. [Colour figure can be viewed at wileyonlinelibrary.com]

While purely geophysical mechanisms without biological involvement can also explain the formation of ridge–runnel bedforms (Whitehouse and Mitchener, 1998; Blanchard *et al.*, 2000; O'Brien *et al.*, 2000; Lanuru *et al.*, 2007; Williams *et al.*, 2008; Carling *et al.*, 2009), evidence for the importance of stabilizing biofilms on the formation and preservation of sedimentary bedforms has accumulated in the past years (e.g. de Boer, 1981; Blanchard *et al.*, 2000; Friend *et al.*, 2008; Noffke, 2010; Weerman *et al.*, 2011; Mariotti *et al.*, 2014). Although the abiotic mechanisms for ridge–runnel formation proposed in previous studies are also essentially scale-dependent feedbacks, the possibility and potential consequences of ridge–runnel self-organization (Yang *et al.*, 2012) have received considerably less scientific attention in the geophysical context than self-organization typically enjoys in the ecosystem sciences. This study shows that regularly patterned algal bedforms are likely formed by self-organization due to scale-dependent feedbacks. This implies that tidal flats can potentially undergo catastrophic shifts between alternative states (e.g. May, 1977; van de Koppel *et al.*, 2001; Scheffer *et al.*, 2012; Weerman *et al.*, 2012; Kéfi *et al.*, 2016; Bastiaansen *et al.*, 2018) and emphasizes the need for the development of models (e.g. Rietkerk *et al.*, 2002, 2004; Guichard *et al.*, 2003; van de Koppel *et al.*, 2005; Kéfi *et al.*, 2007, 2011, 2014; Weerman *et al.*, 2010,

2012; Liu *et al.*, 2012, 2014a; Bastiaansen *et al.*, 2018) to better interpret biogeomorphic changes observed in the field and to help predict possible tipping points.

Persistence of the *Vaucheria* bedforms

Despite morphological and mechanistic similarities between the observed algal bedforms and self-organized diatom patterns (Weerman *et al.*, 2010), the observed *Vaucheria* patterns prove to be long-lived. Both the bedforms and the coinciding algal mats remained in place for multiple years, at least from 2012 to 2016 (Figures 3–5 and SI7), but their development might have already started between 2009 and 2012 and possibly continued until 2017. Although algal cover is strongly reduced in winter and/or during hot and dry periods (visually determined, see Figure SI9), their stabilized topography does persist year-round with little change. This observation might imply that bedform stability is maintained by purely geophysical processes when *Vaucheria* cover is low (e.g. Gouleau *et al.*, 2000; O'Brien *et al.*, 2000; Williams *et al.*, 2008; Carling *et al.*, 2009), or by other (less prominent) algae (Gallagher and Humm, 1981). Viable *Vaucheria* spores are found even in sediment without visible algal cover (Figure SI3). In any case, the observation of flattened bedforms (topographic relief halved in September 2017, as compared to August 2015 and December 2016), seemingly following a temporal shift of *Vaucheria* from ridges to runnels between May and July 2017 (Figure SI9a), seems to support the expectation that biofilms can significantly contribute to bedform formation and maintenance (e.g. de Boer, 1981; Blanchard *et al.*, 2000; Lanuru *et al.*, 2007; Friend *et al.*, 2008; Weerman *et al.*, 2011; Fagherazzi *et al.*, 2013; Mariotti *et al.*, 2014). This disruption of the spatial biostabilization pattern might be short-term, due to disintegration of *Vaucheria* filaments at high temperatures (Gallagher and Humm, 1981), or announcing a critical point in bedform self-organization which is reached when the accretionary mudflat is no longer inundated with sufficient frequency (as observed for stromatolites; Logan, 1961). *Vaucheria*'s known potential to form dense filamentous networks which deeply penetrate the sediment makes it less susceptible to erosion than, say, microbial biofilms that form a 'skin' layer (de Brouwer *et al.*, 2000; Widdows and Brinsley, 2002; Le Hir *et al.*, 2007; Weerman *et al.*, 2011, 2012). Such a 'memory' effect is reflected in the wavy-crinkly laminae observed deep in the sediment (Figures 6 and SI8), and likely contributes to bedform persistence. Long-term biotic effects on the development of sedimentary landscapes have previously been associated mostly with more complex organisms, such as salt marsh plants (e.g. Temmerman *et al.*, 2007; Schwarz *et al.*, 2014). Hence, improved understanding of the long-term biogeomorphic effects of biofilm-like colonization, which is typically much faster and spatially more extensive than plant colonization, is desirable to understand how widespread and relevant this process is in shaping sedimentary landscapes.

Biofilm influence on bedform lamination

This study suggests that ridge lamination becomes more pronounced and microbialite-like due to multi-annual ridge biostabilization by *Vaucheria*, which promotes persistent ridge accretion while introducing a seasonal signal to the

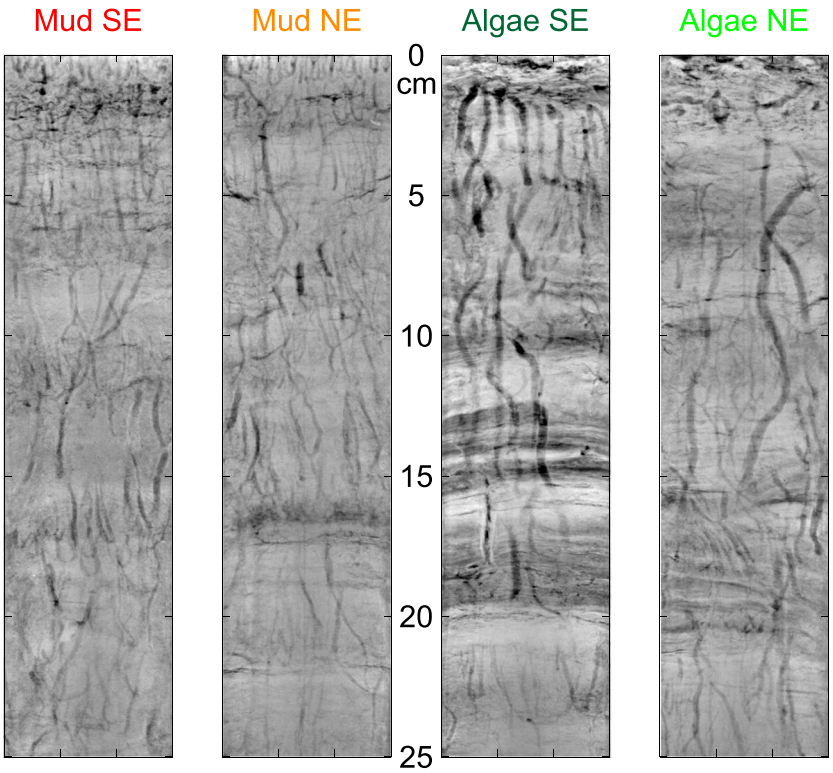

Figure 6. X-radiographs of the sediment cores (6 × 25 cm selection) taken in September 2016 in bare runnels ('mud') and algal-covered creek levees ('algae'), both taken around the northeastern edge (NE) and the southeastern edge (SE) of the Ketenisse focus area (see Figure SI1 for core locations). Background profiles $S_4(x, y)$ have been subtracted to obtain these relative grey intensity profiles. Outliers were determined manually for the collective (four cores) data; all cores are displayed with the same resulting range (i.e. excluding outliers: relative grey intensity between −62 and +40). Broad scale (~4 cm wavelength) and fine scale (less than centimetre scale) horizontal lamination is visible in the algal cores, but less evident in the mud cores. Darker vertical lines are signs of bioturbation. [Colour figure can be viewed at wileyonlinelibrary.com]

sedimentary deposit. X-radiographs of algal-covered creek levee deposits reveal broad light and dark layers, alternating with a spacing roughly equal to annual accretion (Figures 6 and SI4). This probably reflects seasonality in biofilm growth, environmental conditions or both (e.g. Williams *et al.*, 2008). Fine-scale wavy-crinkly laminae (Figures 6 and SI8), indicators of biogenic activity (Horodyski, 1982; Schieber, 1999; Noffke *et al.*, 2007; Riding, 2011; Sarkar *et al.*, 2016), are most evident in darker layers. These crinkle-comprising layers, whose dark colour might reflect lower density associated with porous, felt-like *Vaucheria* mats, are most abundant at depths that likely coincide with the years 2011–2013, in which the strongest algal cover is observed (Figures 3 and 6). Layering is much less evident in bare runnel sediments, despite similar year-averaged accretion rates in runnels and on ridges (or creeks and levees), which is in agreement with earlier studies showing that ridge/levee sediments are more gradually deposited and more (a)biotically stabilized, whereas runnel/creek sediments have higher turnover rates (Blanchard *et al.*, 2000; Gouleau *et al.*, 2000; O'Brien *et al.*, 2000; Lanuru *et al.*, 2007; Williams *et al.*, 2008; Carling *et al.*, 2009; Fagherazzi *et al.*, 2013). Indeed, algal-covered creek levees were found to have significantly higher penetration resistance than bare creek levees and runnels (Figure 7). Although lamination was measured at different moments in time and different locations on the mudflat than penetration resistance, and although the stability contrast might be partly related to the generally higher elevation (and thus lower water content) of algal-covered substrate, these combined measurements strongly suggest a substantial biotic contribution to ridge lamination and stabilization. The fact that lamination is less evident under algal mats closer to the waterfront ('Algae NE' in Figure 6; Figure SI1) might relate to stronger current- and wave-driven disturbances at this lower elevation. Indeed, around the latter location, overall bedform persistence seems shorter (Figure SI2) than around the location of the clearly laminated algal core ('Algae SE'; Figures 4 and 6). As sedimentation patterns are inherently more repetitive in bedforms shaped by a consistent feedback than in bedforms shaped by random disturbances, scale-dependent feedbacks might hence stimulate the formation of laminated deposits.

Resemblance to microbialites and wider implications

This study, combined with existing literature, supports the idea that the observed modern *Vaucheria* bedforms behave in a similar mechanistic and morphologic way to ancient microbialites found in the geological record. The scale-dependent feedback proposed in the current study is comparable to the mechanism described (but not pointed out as feedback) for stromatolites (e.g. Logan, 1961). The observed metre-scale, regular alternation of bare runnels and mat-covered, wavy-crinkly laminated ridges is similar to many layered microbialites (e.g. Logan, 1961; Andres and Reid, 2006; Riding, 2011; Noffke and Awramik, 2013). *Vaucheria* shares many characteristics with organisms known to form microbialites. Flow deceleration, grain trapping and incorporation, and biostabilization (Noffke et al., 2001; Noffke and Awramik, 2013) are known to occur in *Vaucheria* mats (and other biofilms) as well (Black, 1933; Webber, 1967; Simons, 1975; Gallagher and Humm, 1981; Paterson, 1994; Skowroński *et al.*, 1998; Wilcox, 2012). Although these organisms are mainly found in siliciclastic environments, calcification has been observed in freshwater *Vaucheria* mats as well (e.g. Freytet and Verrecchia, 1998; Golubić *et al.*, 2008; Pentecost *et al.*, 2014). Further, fossil algae seemingly morphologically and ecologically equivalent to *Vaucheria* have been found in rocks of Precambrian age (Butterfield, 2004). Finally, *Vaucheria*-covered bedforms can resemble the morphology of dome-shaped stromatolites (Figure 2; but note that this photo dates from before the start of the current study and so no detailed measurements could be done). The photo in Figure 2 suggests that biological processes have contributed strongly to shaping these bedforms: they seem to have steep slopes (suggesting biotic importance; Noffke and Krumbein, 1999) and more complex (not purely flow-shaped) morphologies. Moreover, the domed bedform surfaces suggest that ridges formed by accretion (Carling *et al.*, 2009), different from the tabular elevations that remain when a flat, mat-covered surface is erosively disturbed to form erosional remnants and pockets (Noffke, 1999, 2010; Noffke and Krumbein, 1999). Therefore, the proposed mechanism of biotically stimulated self-organization due to biophysical scale-dependent feedbacks might well explain regularly

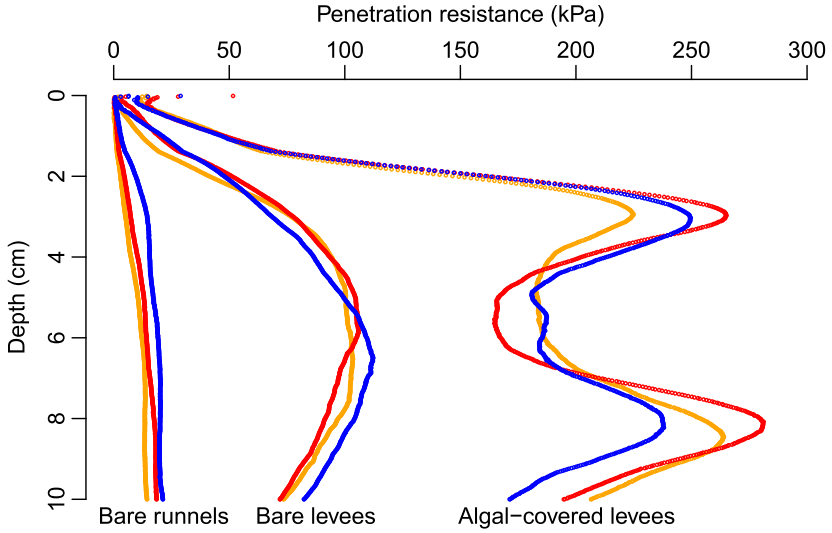

Figure 7. Sediment strength (penetration resistance) vs depth, for three cores taken in bare runnels, bare creek levees and *Vaucheria*-covered creek levees (Ketenisse mudflat, June 2015; see Figure SI1 for sample location). Different colours denote the three different sites sampled for each substrate type, for replication. [Colour figure can be viewed at wileyonlinelibrary.com]

patterned microbialites formed by *Vaucheria* mats and other biofilms, from the Precambrian to present day.

Despite earlier reports on microbialite self-organization (e.g. Petroff *et al.*, 2010; Brasier, 2011; Tice *et al.*, 2011; Bosak *et al.*, 2013 and references cited therein), the potential implications of these findings have not been elaborated on thus far (Purkis *et al.*, 2016). If the bedforms and lamination presented in the current study were preserved in the rock record and used for a geological reconstruction, the feedbacks and self-organization mechanism proposed here may significantly affect such reconstructions (e.g. Purkis *et al.*, 2015). The observed ridge flattening (2017) might be preserved in the rock record as horizontally wider, but vertically thinner (or even absent), ridge layers. Layer thinning might traditionally be explained as the result of an environmental change (e.g. reduced large-scale sediment availability); a missing layer might complicate layer sequence dating and ridge widening might be interpreted as a wavelength increase related to rising water levels (Franca and Lemmin, 2006; Carling *et al.*, 2009). However, the current study suggests that such layer changes could as well be triggered by a disruption of the internal biophysical feedback, leading to bedform broadening while water depth is shoaling (Figures 3, 4, 5, SI2 and SI7), and without the need for changes in external conditions. That is, the changes in layer geometry can be controlled by autogenic as well as allogenic processes (e.g. Purkis *et al.*, 2016). Further study is required to state with more confidence whether the broadening auto-correlation signals (Figures 5 and SI7) truly reflect an increase in the entire bedform wavelength or, instead, reflect ridge widening (runnel narrowing) or the disappearance of single ridges while the rest of the pattern stays intact. System-internal processes such as lateral bedform migration or pattern wavelength multi-stability (Bastiaansen *et al.*, 2018) could also be preserved as a seemingly abrupt change in rock lamination. When using laminated microbialites to interpret, date or correlate between rock records (e.g. Logan *et al.*, 1964; Jerzykiewicz and Sweet, 1988; Ndiaye *et al.*, 2012; Harzhauser *et al.*, 2014) it is therefore important to combine lamination analysis with the use of other proxies (such as stable isotopes) for environmental changes in sea water chemistry, ambient temperature, and so on (Dabkowski *et al.*, 2015; Lettéron *et al.*, 2017). Moreover, the investigated stratigraphic sections should ideally be sampled along a transect of equidistant vertical cores to capture at least one entire microbialite wavelength, as possible changes in bedform wavelength or spanwise location provide valuable information. Finally, combining stratigraphic analyses with mathematical models for (self-organized) microbialite dynamics, such as existing abiotic (Grotzinger and Rothman, 1996) and biotic (Weerman *et al.*, 2010) models, could help to solidify the interpretation.

Conclusions

This study reports on present-day biofilms of filamentous *Vaucheria* algae that stimulate the build-up and maintenance of algal-covered ridges and bare runnels on intertidal flats. These bedforms plausibly self-organize due to local interactions of preferred ridge stabilization and runnel erosion; ridge biostabilization by biofilms most likely amplifies this scale-dependent feedback. Flow deceleration and sediment trapping, binding and stabilization by algal filaments promote wavy-crinkly laminated ridge deposition. The proposed formation processes and observed laminae in – and regular morphologies of – these modern biofilm bedforms may mirror the microbialitic deposits that dominated the shallow-marine landscape as early as the Precambrian. This suggestion of microbialite self-organization may also be important for geological reconstructions based on organosedimentary laminae in Earth's early rock record.

Acknowledgements—The authors thank Aniek van den Berg, Jeroen van Dalen, Lennart van IJzerloo and Bas Oteman for their assistance with fieldwork and analyses and are grateful for the help of Henko C. de Stigter and Rineke Gieles-Witte in making the X-radiographs. The feedback of Huib E. de Swart on earlier versions of the paper has been very valuable. Loreta Cornacchia provided helpful insights into the use of spatial auto-correlations and Evert Jan Bakker into some other statistical analyses. Annette Wielemaker helped with finetuning Figure SI1. The photo used for Figure 2 was kindly provided by Frank Wagemans. The authors thank Nora Noffke and one other (anonymous) reviewer for their valuable feedback.

The research of RCvdV was supported by the programme 'The New Delta' (Project No. 869.15.003) of the Nederlandse Organisatie voor Wetenschappelijk Onderzoek (NWO). JvB was supported by the Vlaams-Nederlandse Scheldecommissie (VNSC) project 'Vegetation modelling HPP' (Contract No. 3109 1805). The authors declare no conflict of interest.

References

Allen JRL. 1987. Streamwise erosional structures in muddy sediments, Severn Estuary, southwestern UK. *Geografiska Annaler: Series A, Physical Geography* **69**(1): 37–46.

Andres MS, Reid RP. 2006. Growth morphologies of modern marine stromatolites: a case study from Highborne Cay, Bahamas. *Sedimentary Geology* **185**(3–4): 319–328.

Atwood TB, Connolly RM, Ritchie EG, Lovelock CE, Heithaus MR, Hays GC, Fourqurean JW, Macreadie PI. 2015. Predators help protect carbon stocks in blue carbon ecosystems. *Nature Climate Change* **5**(12): 1038–1045.

Bastiaansen R, Jaïbi O, Deblauwe V, Eppinga MB, Siteur K, Siero E, Mermoz S, Bouvet A, Doelman A, Rietkerk M. 2018. Multistability of model and real dryland ecosystems through spatial self-organization. *Proceedings of the National Academy of Sciences* **115** (44): 11256–11261.

Black M. 1933. The algal sediments of Andros Island, Bahamas. *Royal Society Philosophical Transactions, Series B* **122**: 169–192.

Blanchard GF, Paterson DM, Stal LJ, Richard P, Galois R, Huet V, Kelly J, Honeywill C, de Brouwer J, Dyer K, Christie M, Seguignes M. 2000. The effect of geomorphological structures on potential biostabilisation by microphytobenthos on intertidal mudflats. *Continental Shelf Research* **20**(10–11): 1243–1256.

Bosak T, Knoll AH, Petroff AP. 2013. The meaning of stromatolites. *Annual Review of Earth and Planetary Sciences* **41**: 21–44.

Brasier MD. 2011. Towards a null hypothesis for stromatolites. In *Earliest Life on Earth: Habitats, Environments and Methods of Detection*, Golding SD, Glikson M (eds). Springer: Dordrecht; 115–125.

Brinkman A, Dankers NMJA, van Stralen M. 2002. An analysis of mussel bed habitats in the Dutch Wadden Sea. *Helgoland Marine Research* **56**(1): 59–75.

Burne RV, Moore LS. 1987. Microbialites: organosedimentary deposits of benthic microbial communities. *Palaios* **2**(3): 241–254.

Butterfield NJ. 2004. A vaucheriacean alga from the middle Neoproterozoic of Spitsbergen: implications for the evolution of Proterozoic eukaryotes and the Cambrian explosion. *Paleobiology* **30**: 231–252.

Cao H, Zhu Z, Balke T, Zhang L, Bouma TJ. 2018. Effects of sediment disturbance regimes on Spartina seedling establishment: implications for salt marsh creation and restoration. *Limnology and Oceanography* **63**(2): 647–659.

Carling PA, Williams JJ, Croudace IW, Amos CL. 2009. Formation of mud ridge and runnels in the intertidal zone of the Severn Estuary, UK. *Continental Shelf Research* **29**(16): 1913–1926.

Chmura GL, Anisfeld SC, Cahoon DR, Lynch JC. 2003. Global carbon sequestration in tidal, saline wetland soils. *Global Biogeochemical Cycles* **17**(4): 1111. https://doi.org/10.1029/2002GB001917.

Christianen MJ, van Belzen J, Herman PM, van Katwijk MM, Lamers LP, van Leent PJ, Bouma TJ. 2013. Low-canopy seagrass beds still provide important coastal protection services. *PloS ONE* **8**(5): e62413.

Cornacchia L, van de Koppel J, van der Wal D, Wharton G, Puijalon S, Bouma TJ. 2018. Landscapes of facilitation: how self-organized patchiness of aquatic macrophytes promotes diversity in streams. *Ecology* **99**(4): 832–847.

Dabkowski J, Royle SH, Antoine P, Marca-Bell A, Andrews JE. 2015. High-resolution $\delta^{18}O$ seasonality record in a French Eemian tufa stromatolite (Caours, Somme Basin). *Palaeogeography, Palaeoclimatology, Palaeoecology* **438**: 277–284.

de Boer PL. 1981. Mechanical effects of micro-organisms on intertidal bedform migration. *Sedimentology* **28**(1): 129–132.

de Brouwer JFC, Bjelic S, de Deckere EMGT, Stal LJ. 2000. Interplay between biology and sedimentology in a mudflat (Biezelingse Ham, Westerschelde, The Netherlands). *Continental Shelf Research* **20** (10–11): 1159–1177.

Du M, Noguchi N. 2017. Monitoring of wheat growth status and mapping of wheat yield's within-field spatial variations using color images acquired from UAV-camera system. *Remote Sensing* **9**(3): 289.

Durán O, Herrmann HJ. 2006. Vegetation against dune mobility. *Physical Review Letters* **97**(18): 188001.

Fagherazzi S, FitzGerald DM, Fulweiler RW, Hughes Z, Wiberg PL, McGlathery KJ, Morris JT, Tolhurst TJ, Deegan LA, Johnson DS. 2013. Ecogeomorphology of tidal flats. In *Ecogeomorphology. Treatise on Geomorphology*, Schroder JE (ed), Vol. **12**. Elsevier: Amsterdam; 201–200.

Fonseca MS. 1989. Sediment stabilization by *Halophila decipiens* in comparison to other seagrasses. *Estuarine, Coastal and Shelf Science* **29**(5): 501–507.

Franca MJ, Lemmin U. 2006. Cross-section periodicity of turbulent gravel-bed river flows. *Proceedings of the 4th River, Coastal, and Estuarine Morphodynamics Conference* **1**: 203–210.

Freytet P, Verrecchia EP. 1998. Freshwater organisms that build stromatolites: a synopsis of biocrystallization by prokaryotic and eukaryotic algae. *Sedimentology* **45**(3): 535–563.

Friend PL, Lucas CH, Holligan PM, Collins MB. 2008. Microalgal mediation of ripple mobility. *Geobiology* **6**(1): 70–82.

Gallagher SB, Humm HJ. 1981. *Vaucheria* (Xanthophyceae, Vaucheriaceae) of the central Florida gulf coast. *Bulletin of Marine Science* **31**(1): 184–190.

Golubić S, Violante C, Plenković-Moraj A, Grgasović T. 2008. Travertines and calcareous tufa deposits: an insight into diagenesis. *Geologia Croatica* **61**(2–3): 363–378.

Gouleau D, Jouanneau JM, Weber O, Sauriau PG. 2000. Short- and long-term sedimentation on Montportail–Brouage intertidal mudflat, Marennes–Oleron Bay (France). *Continental Shelf Research* **20**(12–13): 1513–1530.

Grabowski RC, Droppo IG, Wharton G. 2011. Erodibility of cohesive sediment: the importance of sediment properties. *Earth-Science Reviews* **105**(3–4): 101–120.

Grotzinger JP, Knoll AH. 1999. Stromatolites in Precambrian carbonates: evolutionary mileposts or environmental dipsticks? *Annual Review of Earth and Planetary Sciences* **27**(1): 313–358.

Grotzinger JP, Rothman DH. 1996. An abiotic model for stromatolite morphogenesis. *Nature* **383**(6599): 423–425.

Guichard F, Halpin PM, Allison GW, Lubchenco J, Menge BA. 2003. Mussel disturbance dynamics: signatures of oceanographic forcing from local interactions. *The American Naturalist* **161**(6): 889–904.

Harzhauser M, Peckmann J, Birgel D, Draganits E, Mandic O, Theobalt D, Huemer J. 2014. Stromatolites in the Paratethys Sea during the Middle Miocene climate transition as witness of the Badenian salinity crisis. *Facies* **60**(2): 429–444.

Horodyski RJ. 1982. Impressions of algal mats from the Middle Proterozoic Belt Supergroup, northwestern Montana, USA. *Sedimentology* **29**(2): 285–289.

Hu Z, Belzen J, Wal D, Balke T, Wang ZB, Stive M, Bouma TJ. 2015. Windows of opportunity for salt marsh vegetation establishment on bare tidal flats: the importance of temporal and spatial variability in hydrodynamic forcing. *Journal of Geophysical Research: Biogeosciences* **120**(7): 1450–1469.

James RK, Silva R, van Tussenbroek BI, Escudero-Castillo M, Mariño-Tapia I, Dijkstra HA, van Westen RM, Pietrzak JD, Candy AS, Katsman CA, van der Boog CG, Riva REM, Slobbe C, Klees R, Stapel J, van der Heide T, van Katwijk M, Herman PMJ, Bouma TJ. 2019. Maintaining tropical beaches with seagrass and algae: a promising alternative to engineering solutions. *BioScience* **69**(2): 136–142.

Jerzykiewicz T, Sweet AR. 1988. Sedimentological and palynological evidence of regional climatic changes in the Campanian to Paleocene sediments of the Rocky Mountain Foothills, Canada. *Sedimentary Geology* **59**(1–2): 29–76.

Kearney WS, Fagherazzi S. 2016. Salt marsh vegetation promotes efficient tidal channel networks. *Nature Communications* **7**: 12287.

Kéfi S, Rietkerk M, Alados CL, Pueyo Y, Papanastasis VP, ElAich A, de Ruiter PC. 2007. Spatial vegetation patterns and imminent desertification in Mediterranean arid ecosystems. *Nature* **449**(7159): 213–217.

Kéfi S, Rietkerk M, Roy M, Franc A, de Ruiter PC, Pascual M. 2011. Robust scaling in ecosystems and the meltdown of patch size distributions before extinction. *Ecology Letters* **14**(1): 29–35.

Kéfi S, Guttal V, Brock WA, Carpenter SR, Ellison AM, Livina VN, Seekell DA, Scheffer M, van Nes EH, Dakos V. 2014. Early warning signals of ecological transitions: methods for spatial patterns. *PloS ONE* **9**(3): e92097.

Kéfi S, Holmgren M, Scheffer M. 2016. When can positive interactions cause alternative stable states in ecosystems? *Functional Ecology* **30** (1): 88–97.

Lanuru M, Riethmüller R, van Bernem C, Heymann K. 2007. The effect of bedforms (crest and trough systems) on sediment erodibility on a back-barrier tidal flat of the East Frisian Wadden Sea, Germany. *Estuarine, Coastal and Shelf Science* **72**(4): 603–614.

Le Hir P, Monbet Y, Orvain F. 2007. Sediment erodability in sediment transport modelling: can we account for biota effects? *Continental Shelf Research* **27**(8): 1116–1142.

Lettéron A, Fournier F, Hamon Y, Villier L, Margerel JP, Bouche A, Feist M, Joseph P. 2017. Multi-proxy paleoenvironmental reconstruction of saline lake carbonates: paleoclimatic and paleogeographic implications (Priabonian-Rupelian, Issirac Basin, SE France). *Sedimentary Geology* **358**: 97–120.

Liu QX, Weerman EJ, Herman PM, Olff H, van de Koppel J. 2012. Alternative mechanisms alter the emergent properties of self-organization in mussel beds. *Proceedings of the Royal Society, Series B* **279**(1739): 2744–2753.

Liu QX, Weerman EJ, Gupta R, Herman PM, Olff H, van de Koppel J. 2014a. Biogenic gradients in algal density affect the emergent properties of spatially self-organized mussel beds. *Journal of The Royal Society Interface* **11**(96): 20140089.

Liu QX, Herman PM, Mooij WM, Huisman J, Scheffer M, Olff H, van de Koppel J. 2014b. Pattern formation at multiple spatial scales drives the resilience of mussel bed ecosystems. *Nature Communications* **5**: 5234.

Logan BW. 1961. Cryptozoon and associate stromatolites from the Recent, Shark Bay, Western Australia. *Journal of Geology* **69**(5): 517–533.

Logan BW, Rezak R, Ginsburg RN. 1964. Classification and environmental significance of algal stromatolites. *Journal of Geology* **72**(1): 68–83.

Mariotti G, Perron JT, Bosak T. 2014. Feedbacks between flow, sediment motion and microbial growth on sand bars initiate and shape elongated stromatolite mounds. *Earth and Planetary Science Letters* **397**: 93–100.

May RM. 1977. Thresholds and breakpoints in ecosystems with a multiplicity of stable states. *Nature* **269**(5628): 471–477.

McLeod E, Chmura GL, Bouillon S, Salm R, Björk M, Duarte CM, Lovelock CE, Schlesinger WH, Silliman BR. 2011. A blueprint for blue carbon: toward an improved understanding of the role of vegetated coastal habitats in sequestering CO_2. *Frontiers in Ecology and the Environment* **9**(10): 552–560.

Ndiaye M, Davaud EJ, Ariztegui D, Fall M. 2012. A semi automated method for laminated sediments analysis. *International Journal of Geosciences* **3**(01): 206–210.

Neumeier U, Ciavola P. 2004. Flow resistance and associated sedimentary processes in a Spartina maritima salt-marsh. *Journal of Coastal Research* **20**(2): 435–447.

Newell RI, Koch EW. 2004. Modeling seagrass density and distribution in response to changes in turbidity stemming from bivalve filtration and seagrass sediment stabilization. *Estuaries* **27**(5): 793–806.

Noffke N. 1999. Erosional remnants and pockets evolving from biotic–physical interactions in a Recent lower supratidal environment. *Sedimentary Geology* **123**(3–4): 175–181.

Noffke N. 2008. Turbulent lifestyle: microbial mats on Earth's sandy beaches – today and 3 billion years ago. *GSA Today* **18**(10): 4–9. https://doi.org/10.1130/GSATG7A.1.

Noffke N. 2010. *Geobiology: Microbial Mats in Sandy Deposits from the Archean Era to Today*. Springer Science & Business Media: Berlin.

Noffke N, Awramik SM. 2013. Stromatolites and MISS – differences between relatives. *GSA Today* **23**(9): 4–9.

Noffke N, Krumbein WE. 1999. A quantitative approach to sedimentary surface structures contoured by the interplay of microbial colonization and physical dynamics. *Sedimentology* **46**(3): 417–426.

Noffke N, Gerdes G, Klenke T, Krumbein WE. 2001. Microbially induced sedimentary structures: a new category within the classification of primary sedimentary structures. *Journal of Sedimentary Research* **71**(5): 649–656.

Noffke N, Beukes N, Bower D, Hazen RM, Swift DJP. 2007. An actualistic perspective into Archean worlds – (cyano-)bacterially induced sedimentary structures in the siliciclastic Nhlazatse Section, 2.9 Ga Pongola Supergroup, South Africa. *Geobiology* **6** (1): 5–20.

Noffke N, Christian D, Wacey D, Hazen RM. 2013. Microbially induced sedimentary structures recording an ancient ecosystem in the ca. 3.48 billion-year-old Dresser Formation, Pilbara, Western Australia. *Astrobiology* **13**(12): 1103–1124.

O'Brien DJ, Whitehouse RJS, Cramp A. 2000. The cyclic development of a macrotidal mudflat on varying timescales. *Continental Shelf Research* **20**(12–13): 1593–1619.

Pascual M, Guichard F. 2005. Criticality and disturbance in spatial ecological systems. *Trends in Ecology & Evolution* **20**(2): 88–95.

Paterson DM. 1989. Short-term changes in the erodibility of intertidal cohesive sediments related to the migratory behavior of epipelic diatoms. *Limnology and Oceanography* **34**(1): 223–234.

Paterson DM. 1994. Microbiological mediation of sediment structure and behaviour. In *Microbial Mats*, Stal LJ, Caumette P (eds). Springer: Berlin; 97–109.

Pentecost A, Merritt R, Carter C. 2014. Growth and calcification of Vaucheria (Xanthophyta) on a travertine surface in a temperate freshwater setting. *European Journal of Phycology* **49**(4): 516–525.

Pestrong R. 1969. The shear strength of tidal marsh sediments. *Journal of Sedimentary Research* **39**(1): 322–326.

Petroff AP, Sim MS, Maslov A, Krupenin M, Rothman DH, Bosak T. 2010. Biophysical basis for the geometry of conical stromatolites. *Proceedings of the National Academy of Sciences* **107**(22): 9956–9961.

Purkis SJ, Casini G, Hunt D, Colpaert A. 2015. Morphometric patterns in Modern carbonate platforms can be applied to the ancient rock record: similarities between Modern Alacranes Reef and Upper Palaeozoic platforms of the Barents Sea. *Sedimentary Geology* **321**: 49–69.

Purkis SJ, van de Koppel J, Burgess PM. 2016. Spatial self-organization in carbonate depositional environments. *SEPM Special Publication* **106**: 53–66.

Raffaelli D, Balls P, Way S, Patterson IJ, Hohmann S, Corp N. 1999. Major long-term changes in the ecology of the Ythan estuary, Aberdeenshire, Scotland; how important are physical factors? *Aquatic Conservation: Marine and Freshwater Ecosystems* **9**(2): 219–236.

Riding R. 2000. Microbial carbonates: the geological record of calcified bacterial–algal mats and biofilms. *Sedimentology* **47**: 179–214.

Riding R. 2011. Microbialites, stromatolites, and thrombolites. In *Encyclopedia of Geobiology*, Reitner J, Thiel V (eds). Springer: Heidelberg; 635–654.

Rietkerk M, van de Koppel J. 2008. Regular pattern formation in real ecosystems. *Trends in Ecology & Evolution* **23**(3): 169–175.

Rietkerk M, Boerlijst MC, van Langevelde F, HilleRisLambers R, van de Koppel J, Kumar L, Prins HHT, de Roos AM. 2002. Self-organization of vegetation in arid ecosystems. *The American Naturalist* **160**(4): 524–530.

Rietkerk M, Dekker SC, de Ruiter PC, van de Koppel J. 2004. Self-organized patchiness and catastrophic shifts in ecosystems. *Science* **305** (5692): 1926–1929.

Romano C, Widdows J, Brinsley MD, Staff FJ. 2003. Impact of *Enteromorpha intestinalis* mats on near-bed currents and sediment dynamics: flume studies. *Marine Ecology Progress Series* **256**: 63–74.

Sarkar S, Choudhuri A, Mandal S. 2016. Microbial mat-related structures shared by both siliciclastic and carbonate formations. *Journal of Palaeogeography* **5**: 278–291.

Scheffer M, Carpenter SR, Lenton TM, Bascompte J, Brock W, Dakos V, van de Koppel J, van de Leemput IA, Levin SA, van Nes EH, Pascual M, Vandermeer J. 2012. Anticipating critical transitions. *Science* **338** (6105): 344–348.

Schieber J. 1999. Microbial mats in terrigenous clastics; the challenge of identification in the rock record. *Palaios* **14**(1): 3–12.

Schwarz C, Ye QH, van der Wal D, Zhang LQ, Bouma T, Ysebaert T, Herman PMJ. 2014. Impacts of salt marsh plants on tidal channel initiation and inheritance. *Journal of Geophysical Research: Earth Surface* **119**(2): 385–400.

Simons J. 1975. Vaucheria species from estuarine areas in the Netherlands. *Netherlands Journal of Sea Research* **9**(1): 1–23.

Skowroński T, de Knecht JA, Simons J, Verkleij JAC. 1998. Phytochelatin synthesis in response to cadmium uptake in *Vaucheria* (Xanthophyceae). *European Journal of Phycology* **33**(1): 87–91.

Stal LJ. 2010. Microphytobenthos as a biogeomorphological force in intertidal sediment stabilization. *Ecological Engineering* **36**(2): 236–245.

Stal LJ, Caumette P (eds). 1994. *Microbial Mats: Structure, Development and Environmental Significance*, Vol. **35**. Springer Science & Business Media: Berlin.

Sutherland TF, Amos CL, Grant J. 1998. The effect of buoyant biofilms on the erodibility of sublittoral sediments of a temperate microtidal estuary. *Limnology and Oceanography* **43**(2): 225–235.

Temmerman S, Bouma TJ, van de Koppel J, van der Wal D, de Vries MB, Herman PMJ. 2007. Vegetation causes channel erosion in a tidal landscape. *Geology* **35**(7): 631–634.

Tice MM, Thornton DC, Pope MC, Olszewski TD, Gong J. 2011. Archean microbial mat communities. *Annual Review of Earth and Planetary Sciences* **39**: 297–319.

Turing AM. 1952. The chemical basis of morphogenesis. *Philosophical Transactions of the Royal Society of London, Series B* **237**(641): 37–72.

van Belzen J. 2018. Qualitative growth potential test for brackish Vaucheria species. *Protocol Exchange*. https://doi.org/10.1038/protex.2018.041.

van de Koppel J, Herman PM, Thoolen P, Heip CH. 2001. Do alternate stable states occur in natural ecosystems? Evidence from a tidal flat. *Ecology* **82**(12): 3449–3461.

van de Koppel J, Rietkerk M, Dankers N, Herman PM. 2005. Scale-dependent feedback and regular spatial patterns in young mussel beds. *The American Naturalist* **165**(3): E66–E77.

van den Neucker T, Verbessem I, van Braeckel A, Stevens M, Spanoghe G, Gyselings R, Soors J, de Regge N, de Belder J, van den Bergh E. 2007. *Evaluatie van natuurontwikkelingsprojecten in het Scheldeestuarium*. Rapport van het Instituut voor Natuur-en Bosonderzoek.

van der Heide T, van Nes EH, Geerling GW, Smolders AJ, Bouma TJ, van Katwijk MM. 2007. Positive feedbacks in seagrass ecosystems: implications for success in conservation and restoration. *Ecosystems* **10**(8): 1311–1322.

Walter MR, Heys GR. 1985. Links between the rise of the Metazoa and the decline of stromatolites. *Precambrian Research* **29**(1–3): 149–174.

Webber EE. 1967. Bluegreen algae from a Massachusetts salt marsh. *Bulletin of the Torrey Botanical Club* **94**(2): 99–106.

Weerman EJ, van de Koppel J, Eppinga MB, Montserrat F, Liu QX, Herman PM. 2010. Spatial self-organization on intertidal mudflats through biophysical stress divergence. *The American Naturalist* **176** (1): E15–E32.

Weerman EJ, Herman PM, van de Koppel J. 2011. Top-down control inhibits spatial self-organization of a patterned landscape. *Ecology* **92** (2): 487–495.

Weerman EJ, van Belzen J, Rietkerk M, Temmerman S, Kéfi S, Herman PMJ, van de Koppel J. 2012. Changes in diatom patch-size

distribution and degradation in a spatially self-organized intertidal mudflat ecosystem. *Ecology* **93**(3): 608–618.
Whitehouse RJ, Mitchener HJ. 1998. Observations of the morphodynamic behaviour of an intertidal mudflat at different timescales. *Geological Society, London, Special Publications* **139**(1): 255–271.
Whitehouse RJS, Bassoullet P, Dyer KR, Mitchener HJ, Roberts W. 2000. The influence of bedforms on flow and sediment transport over intertidal mudflats. *Continental Shelf Research* **20**(10–11): 1099–1124.
Widdows J, Brinsley M. 2002. Impact of biotic and abiotic processes on sediment dynamics and the consequences to the structure and functioning of the intertidal zone. *Journal of Sea Research* **48**(2): 143–156.
Widdows J, Lucas JS, Brinsley MD, Salkeld PN, Staff FJ. 2002. Investigation of the effects of current velocity on mussel feeding and mussel bed stability using an annular flume. *Helgoland Marine Research* **56**(1): 3–12.
Widdows J, Blauw A, Heip CHR, Herman PMJ, Lucas CH, Middelburg JJ, Schmidt S, Brinsley MD, Twisk F, Verbeek H. 2004. Role of physical and biological processes in sediment dynamics of a tidal flat in Westerschelde Estuary, SW Netherlands. *Marine Ecology Progress Series* **274**: 41–56.
Wilcox MD. 2012. Occurrence of the marine yellow-green algae Vaucheria velutina C. Agardh and Vaucheria longicaulis Hoppaugh (Xanthophyceae: Vaucheriaceae) in Auckland, New Zealand. *New Zealand Journal of Marine and Freshwater Research* **46**(2): 285–290.
Williams JJ, Carling PA, Amos CL, Thompson C. 2008. Field investigation of ridge–runnel dynamics on an intertidal mudflat. *Estuarine, Coastal and Shelf Science* **79**(2): 213–229.
Yang SQ, Tan SK, Wang XK. 2012. Mechanism of secondary currents in open channel flows. *Journal of Geophysical Research: Earth Surface* **117**(F4): F04014. https://doi.org/10.1029/2012JF002510.

Supporting Information

Additional supporting information may be found online in the Supporting Information section at the end of the article.

Figure SI1 – **(a)** Overview of study site locations Ketenisse (K), Galgeschoor (G) and Paardenschor (P), close to the Belgian harbour of Antwerp (A); **(b)** Digital elevation model (m above NAP; laserscan-derived) of Ketenisse (13 December 2016); **(c)** Aerial image (23 July 2012) of Ketenisse. The white rectangle indicates the 44 × 49.5 m focus area; the white dot is the central location of core sampling for the penetration resistance measurements (Figure 7); red resp. blue dots are locations where the two north-eastern resp. south-eastern X-radiograph cores were sampled (Figure 6). Aerial images in figure **(a)** obtained and adapted from Google Earth Pro, © 2016 Google Inc (see photo source along the bottom of this figure). Aerial image in figure **(b)** and **(c)** taken by the Agentschap voor Geografische Informatie Vlaanderen ("Orthofoto's, middenschalig, kleur 2012, Vlaanderen"). Figure SI1 was composed using ArcGIS (ESRI).

Figure SI2 – Bottom elevation profiles along the northern edge of the 44 × 49.5 m focus area on Ketenisse. Elevations derived from in-situ laserscan measurements; NAP roughly is mean sea level. Different lines denote different moments in time at which the elevation was measured. The bedform pattern is less persistent than on the southern edge of the focus area (Figure 4).

Figure SI3 – *Vaucheria* growth potential test for Paardenschor and Ketenisse (see Figure SI1 for study sites). Each bar shows the percentage of samples (5 replicates each) tested positive for *Vaucheria* growth. On Paardenschor, samples were taken in visually bare sediment at three different elevation ranges. On Ketenisse, samples were taken within bare creeks and on bare mudflat. Samples for positive controls were taken in clearly algal-covered sediments. Negative controls (sterilised sediments) always showed 0% growth potential, as required.

Figure SI4 – Spatial auto-correlations along the vertical axis of the relative X-radiographs (Figure 6), after regridding the data to 1 mm resolution. White markers indicate non-significant data points ($p \geq 0.01$), coloured markers are statistically significant ($p < 0.01$) based on 100 random permutations. Each correlation profile is afterwards normalised by dividing it by its maximum value, for visibility.

Figure SI5 – Regularly spaced and elongated algal mat patterns on Paardenschor (51.334521°N, 4.251750°E). Algal mats (2009) become colonised by higher vegetation later on (visible on photos from 2012 onwards). Aerial images © 2018 DigitalGlobe, obtained and adapted from Google Earth Pro, © 2016 Google Inc.

Figure SI7 – Normalised spatial auto-correlations **(a)** and cross-correlations **(b)** of relative green intensity (VDVI) derived from Google Earth images from 2012, 2013, 2015 and 2017, computed along the cross-flow (west–east) direction within the 44 × 49.5 m focus area on Ketenisse. White markers indicate non-significant data points ($p \geq 0.01$), coloured markers are statistically significant ($p < 0.01$) based on 100 random permutations. Each correlation profile is afterwards normalised by dividing it by its maximum value, for visibility.

Figure SI8 - Close-up image between 11.6 and 16.3 cm depth in the "Algae SE" core in Figure 6, revealing wavy-crinkly laminae (examples indicated by arrows). This image is derived from the unprocessed X-radiograph, i.e. with the original 0.085 mm resolution and without subtraction of the background profiles (which was done to obtain Figures 6 and SI4).

Figure SI9 - Bedforms and algal distribution close to the 44 × 49.5 m focus area on Ketenisse, **(a)** during dry and hot summer conditions (15 June 2017) when the algal cover temporarily shifted from the ridges (on the photo: now greyish and elevated) to the sides of the runnels (now greenish and low-lying), and **(b)** during cold winter conditions (8 February 2018) when algal cover is not detectable. Some runnels are filled with ice. Photo (b) taken by Jeroen van Dalen.

Data S1 Supporting information

